The transition from explosive to effusive eruptive regime:
The example of the 1912 Novarupta eruption, Alaska

Nancy K. Adams[†]
Bruce F. Houghton
Sarah A. Fagents
Department of Geology and Geophysics, University of Hawaii, 1680 East-West Road, Honolulu, Hawaii 96822, USA

Wes Hildreth
Volcano Hazards Program, U.S. Geological Survey, Middlefield Road, Menlo Park, California 94025, USA

ABSTRACT

The shift from explosive to effusive silicic volcanism seen in many historical eruptions reflects a change in the style of degassing of erupted magma. This paper focuses on such a transition during the largest eruption of the twentieth century, the 1912 eruption of Novarupta. The transition is recorded in a dacite block bed, which covers an elliptical area of 4 km² around the vent. Approximately 700 studied blocks fall into four main lithologic categories: (1) pumiceous, (2) dense, (3) flow-banded dacites, and (4) welded breccias. Textural analyses of the blocks indicate portions of the melt underwent highly variable degrees of outgassing. Vesicle populations show features characteristic of bubble coalescence and collapse. A decrease in measured vesicularity and increased evidence for bubble collapse compared with pumice from earlier Plinian episodes mark the transition from closed- to open-system degassing. Block morphology and textures strongly suggest the magma was first erupted as a relatively gas-rich lava dome/plug, but incomplete outgassing led to explosive disruption. Heterogeneous degassing of ascending magma began in Plinian Episode III and resulted in instability during Episode IV dome growth and a (series of) Vulcanian explosion(s). Modeling of the dynamics of explosion initiation and ejecta dispersal indicates that a significant concentration in gas is required to produce the explosions responsible for the observed block field dispersal. The amount of gas available in the hot pumiceous dome material appears to have been inadequate to drive the explosion(s); therefore, external water most likely contributed to the destruction.

Keywords: lava domes, plugs, vesicles, microtextures, bubble collapse, decoupled degassing, Novarupta 1912.

INTRODUCTION

Current models link silicic explosive and effusive volcanism to two contrasting patterns of magma ascent and degassing (Jaupart, 1996; Massol and Jaupart, 1999; Melnik, 2000). Explosive eruptions have been characterized by closed-system degassing, in which rapid, coupled ascent of gases and melt leads to late-stage and often disequilibrium release of dissolved volatiles (Mangan and Sisson, 2000; Mangan et al., 2004). Thermodynamic and chemical disequilibrium occurs when the rate in which volatiles can exsolve is exceeded by the rate of magma ascent, which causes a supersaturation of volatiles in the melt (Cashman et al., 2000; Mangan and Sisson, 2000). Effusive eruptions are characterized by open-system degassing, where efficient decoupling of volatiles and melt during ascent in the conduit permits permeable flow and subsequent gas loss to the conduit walls (Jaupart and Allegre, 1991; Jaupart, 1998; Melnik and Sparks, 2002). Eruptions that show explosive-effusive transitions are therefore particularly useful for understanding the switch between closed- and open-system behavior, i.e., coupling versus decoupling of melt and exsolved gas phases.

The 1980–1986 eruption of Mount St. Helens is an example of an intensely studied volcanic system that made the transition from Plinian explosions to dome effusion (Swanson, 1990). After the catastrophic events of 18 May 1980, two domes formed in late June and early August, but were explosively destroyed in late July and mid-October, respectively. Between October 1980 and 1986, a stable dacite dome grew in a complex series of extrusions, producing ~20 lobes (Moore et al., 1981; Swanson et al., 1987; Anderson and Fink, 1989; Fink et al., 1990; Swanson and Holcomb, 1990; Anderson et al., 1995). Here, we describe indirect evidence for a similar transition during the largest twentieth-century eruption at Novarupta, Alaska, in 1912. New field and laboratory data suggest that prior to effusion of the late-stage rhyolitic dome at Novarupta (Episode V of Houghton et al., 2004), the system erupted a short-lived dacite dome or plug (Episode IV) chemically identical to melt erupted explosively in episodes II and III. The nonsurvival of this lava, which we infer was destroyed by a succession of discrete, powerful Vulcanian explosions, reflects the incomplete and spatially variable pattern of outgassing in the last dacitic melt to reach the vent during the 1912 eruption. Such transitions mark a fundamental shift in eruptive regime thought to be driven by a unidirectional shift from closed- to open-system degassing.

A block bed created by the disruption of the Episode IV dacite dome is the focus of this paper. We approached this study on three fronts. First, we described the dispersal area of the block bed and block lithologies based on two weeks of intensive field work. Second, we performed microscopic textural analysis on

[†]E-mail: nanadams@soest.hawaii.edu.

juvenile eruption products to determine ascent and vesiculation patterns. Third, we applied a model of Vulcanian explosion dynamics to better understand the volatile requirements for dome disruption and ejection. Based on these three lines of data, the internal changes of the dacite magma during ascent and degassing can be related to a progression of eruptive regimes from Plinian to effusion to Vulcanian.

BACKGROUND

Explosive and Effusive Behavior

Eruptions involving water-rich silicic magmas often follow complex cycles involving different dynamical regimes, i.e., violent explosive phases as well as effusive dome formation. The shift from explosive to effusive eruption is linked to a change in behaviors from closed- to open-system degassing (Eichelberger et al., 1986; Jaupart and Allegre, 1991; Eichelberger, 1995; Jaupart, 1996). This change is in turn linked to first-order factors, e.g., ascent rate, leading to predictions of sudden, drastic transitions between explosive and effusive eruption (Woods and Koyaguchi, 1994). Data from recent eruptions suggest that the shift between open- and closed-system behavior is complex and involves nonlinear feedbacks between overpressure, ascent rate, magma viscosity, vesiculation, microlite crystallization, and gas loss (Melnik and Sparks, 1999, 2002; Barmin et al., 2002). The microtextures of the eruption products, particularly those formed during the period of transition from explosive to effusive behavior, should therefore preserve evidence of this complex process.

Microtextures

The intricate patterns of magma ascent and degassing during dome growth can be studied via textures of the eruption products. Clast morphology, vesicle size distribution, vesicle shape, and abundance of microlites can be quantified and compared with experimental data (Cashman and Mangan, 1994; Mangan and Cashman, 1996; Gardner et al., 1999; Mangan and Sisson, 2000; Klug et al., 2002; Mangan et al., 2004). When domes have been explosively disrupted, the ejected blocks can be subdivided based on lithology; ultimately the size and textural composition of the parent extrusion can be reconstructed. Scanning electron microscope (SEM)

and scanned images from polished thin sections can be used to quantify microtextural features and to compare vesicularity and crystallinity among the different eruption products. The size distributions of vesicles can constrain the relative timing of processes of nucleation, growth, coalescence, and collapse of bubbles in eruptions and may be used to understand how the style, timing, and extent of magmatic degassing influence ensuing eruptive behavior (Mangan et al., 1993; Cashman and Mangan, 1994; Polacci et al., 2003). Vesicle size distributions commonly do not follow the linear trends seen in crystal populations that result from steady-state nucleation and growth (Cashman and Marsh, 1988; Marsh, 1988; Cashman, 1992), but instead indicate complex histories of magma ascent and degassing (Toramaru, 1990; Cashman and Mangan, 1994; Klug and Cashman, 1994; Mangan and Cashman, 1996). In this study, we focus on the 1912 eruption of Novarupta and use textures of different lithologies from the Episode IV products to trace the transition from closed- to open-system degassing.

The 1912 Eruption

The eruption of Novarupta on 6–8 June 1912 was the largest eruption of the twentieth century, producing ~11 km^3 of ignimbrite and ~17 km^3 of Plinian fall deposits in ~60 h (Hildreth, 1983, 1987). Three episodes of explosive activity produced a succession of Plinian fall deposits and ignimbrite (Fierstein and Hildreth, 1992). For many years, the prevailing thought was that the Plinian phase ended with a sharp transition to the passive extrusion of the late-stage rhyolite dome now preserved at Novarupta (Curtis, 1968; Hildreth, 1983). Recent work has recognized that this final episode (Episode V) of stable dome growth was preceded by eruption and disruption of a dacitic dome or plug at the same site (Hildreth and Fierstein, 2000; Houghton et al., 2004). The Episode IV lava was entirely destroyed by explosive activity and is now represented only by a block and lapilli apron surrounding the Episode V dome.

Lack of caldera collapse at the 1912 vent has preserved three concentric, nested structures at the Novarupta vent region: the crater, the ejecta ring, and the Episode V dome. The crater is a 2-km-wide depression inferred to be the surface expression of a funnel-shaped flaring vent formed during Episode I (Fierstein and Hildreth, 1992). The ejecta ring encloses the current

dome, which is 380 m wide and 65 m high (Hildreth, 1983; Hildreth and Fierstein, 2000). In an ~4 km^2 area surrounding the vent that includes the ejecta ring and extends beyond the southern boundary of the crater, an apron of decimeter- to meter-sized Episode IV dacite blocks overlies the fine ash deposited at the close of Episode III (Fig. 1). Episode IV therefore represents the transition between explosive activity (Episode III) and extrusion of a long-lived dome (Episode V), and as such, the distribution and products of the Episode IV block bed will be the focus of this study.

THE EPISODE IV BLOCK BED

Field Methods

Block Size and Distribution

The distribution of blocks was mapped over 10 d of field work in July 2003. Approximately 690 large blocks were mapped in a rough grid with spacings of 10–30 m according to concentration. Documenting a block included marking its position with two kinematic global positioning system (GPS) units, measuring maximum, minimum, and intermediate diameters, recording texture and lithology, and collecting a representative sample. A significant number of blocks broke into many pieces upon impact; the point of impact could generally be discerned from the fan-shaped dispersal of the clasts. In such cases, the fragments were fitted together like pieces in a puzzle to reconstruct the dimensions of the original block, and the dimensions of the largest piece were also measured (Fig. 2B). When the comminution of the block was extensive and pre-impact block morphology was impossible to ascertain, pieces were gathered into a pile, and its dimensions measured (Fig. 2C). Error introduced by this method was assessed in the laboratory using the following procedure. A block of Styrofoam with known dimensions was carved into >20 pieces. The pieces were shuffled, then gathered into a pile, and dimensions were measured ten times (Fig. 2D). The average dimension of each pile was 51 ± 3% greater than the original block; thus, the average dimensions of piles measured in the field were scaled down accordingly. ArcGIS by ESRI was used to create maps showing block distribution. GPS locations for each block and aerial photos were coregistered to 15 min Alaska digital elevation model (DEM) data and Arc vector files of
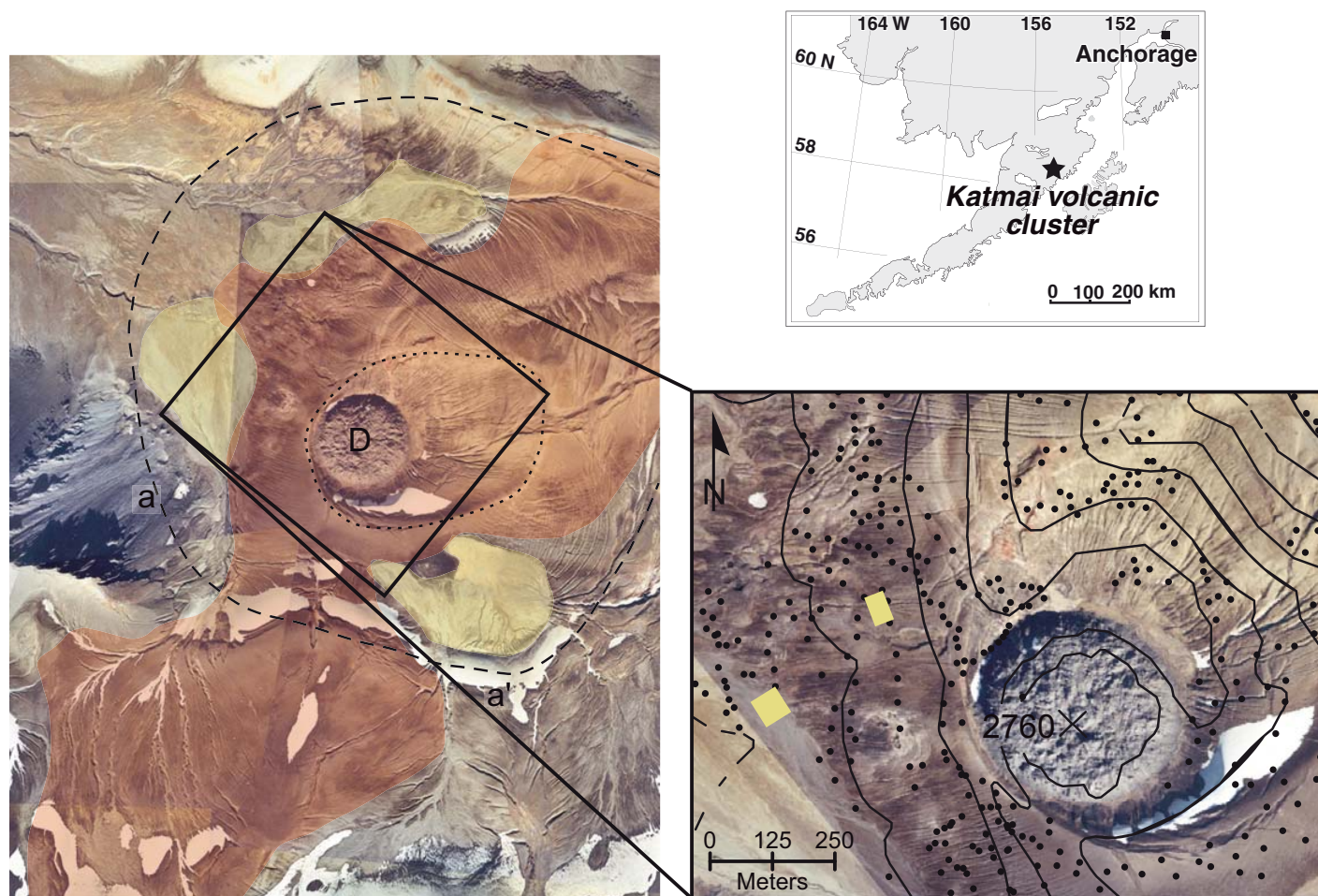
Figure 1. (Left) Aerial photo mosaic of Novarupta vent region. Ejecta ring is delineated by dotted line; crater rim is traced by dashed line. Features include current dome (D), alluvial fans (yellow), and steep crater wall (a–a′). Area covered by block bed and mapped is highlighted in red. (Bottom right) Topographic contours (interval = 100 ft) superimposed on enlarged rectangle. Black dots mark positions of mapped blocks. The 60 × 40 m and 60 × 60 m areas used for the component studies are shown in yellow. (Top right) Map of the Alaskan peninsula showing the location of the Katmai group volcanoes.

topographic maps for U.S. Geological Survey Mt. Katmai quadrangles.

Block Componentry

The blocks are dacitic in composition but have a wide range of textures and lithologies and include pumiceous and dense dacites and breccias (Fig. 3). Many of the blocks were apparently ejected at high temperatures; breadcrust textures are present among all lithologies (Figs. 2B, 3C). Flow-banding is also common and exists over a range of vesicularities (Fig. 3D). Pumiceous and dense dacites were considered juvenile material, i.e., they were newly erupted during Episode IV. The origin of the breccias is more complex. A small portion of the densely welded breccias, or vitrophyres, contains pieces of pre-1912 wall rock;

these breccias were classified as nonjuvenile. Lightly and moderately welded breccias, however, appear mostly monolithic; crystal-rich pumice clasts are set in a matrix of similarly vesiculated ash- to lapilli-sized material. These breccias probably originated as part of the dome/plug carapace but had equilibrated thermally with atmospheric temperatures. Recording lithology consisted of assigning the block to a textural category, estimating degree of vesicularity and crystallinity, and noting the presence of flow bands and bread-crust textures. If the block was a breccia, the degree of welding was observed, and for flow-banded blocks, the type of banding was described. Ultimately, blocks were grouped into breccias, pumiceous dacites, dense dacites, and flow-banded dacites. Breccias were subdivided

into lightly, moderately, and densely welded categories, and flow-banded blocks were split into pumiceous, dense, and mixed (mingled pumiceous and dense bands) types. Pieces of blocks were taken at the time of recording and grouped to form samples from each textural subgroup. The number of specimens per subgroup necessarily reflected their relative abundance within the block bed.

To conduct a large-scale componentry exercise, the 100 largest blocks in two fixed areas were counted, measured, and grouped texturally at sites 450 and 608 m west of the center of the Episode V dome (Fig. 1). The sites were chosen for their relatively flat slope, remote position from drainages and runoff-influenced zones, and moderate concentration of blocks. Northwest-southeast swaths were then made in which
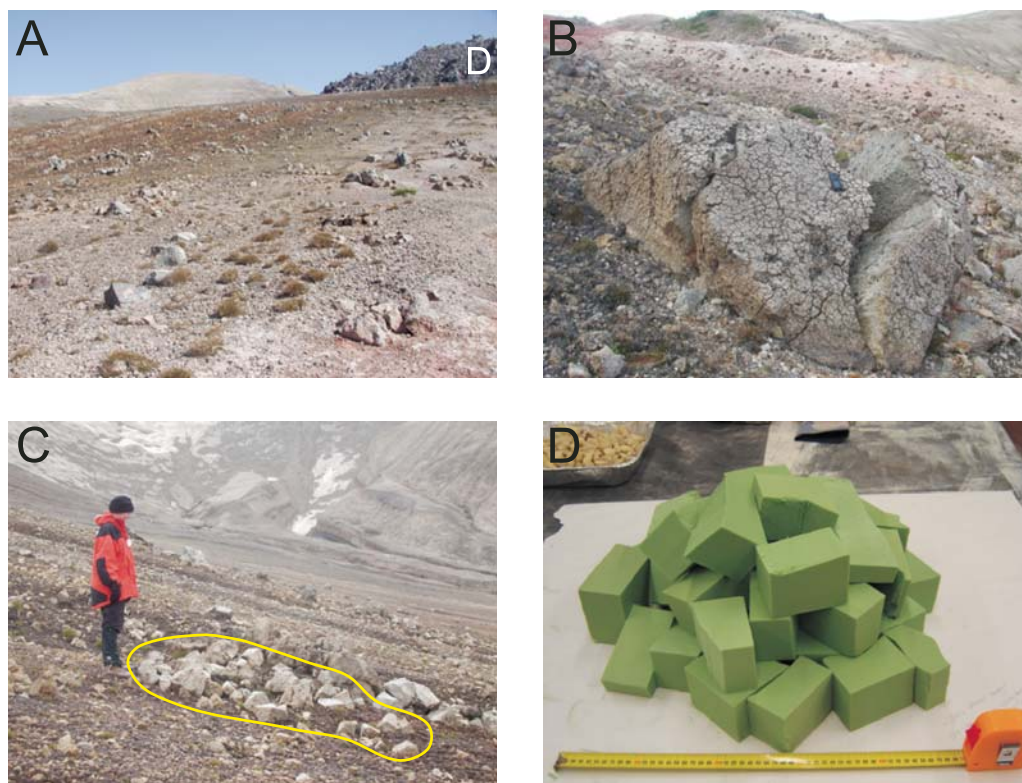
Figure 2. Approximately 700 blocks were mapped for this study. (A) Out-sized and often broken blocks lie directly on fine ash; Episode V dome is in background (white D). (B) Many blocks broke upon impact, but the pieces fit together like a puzzle. (C) Comminution of some blocks was too severe for reconstruction; dispersal boundary of individual block pieces is marked by yellow line. (D) Pile method used when blocks were too broken to reconstruct along original dimensions (as in C) was assessed in the laboratory for error.

Figure 3. Blocks showed a range of lithologies and surface textures. (A) Pumiceous dacite block characterized by coarse vesicles. (B) Bread-crusted breccia block. (C) The original dimensions of this highly fractured, bread-crusted dense dacite block remain discernable after impact. (D) Mixed flow-banded block of pumiceous and dense dacite.

every major block was counted until a total of 100 blocks was reached. Collectively, the swaths defined 60 × 60 m and 60 × 40 m rectangles.

Distribution of Ejecta

Data

Isolated individual blocks up to 12 m³ in volume or 10⁴ kg in mass form a 4 × 2 km elliptical apron with a N-S dispersal axis (Fig. 1). The blocks overlie the Layer H ash deposited at the close of Episode III (Fig. 2A); in places, the blocks also overlie thin deposits of fluvially and slope-reworked pumice, implying that a short time break occurred after the close of the main explosive phase of the 1912 eruption. There are two reasons that the blocks are inconspicuous in certain sectors within a 0.5–1.5 km radius of the current dome: (1) The blocks are buried by modern alluvial fans south and west of the

vent (yellow on Fig. 1), and (2) on the steep inner wall of the crater southwest of Novarupta, blocks landed but then rolled to accumulate at the break in slope (a–a′ on Fig. 1).

We assessed distribution by block size according to (1) the average dimension of the whole or reconstructed block ($\overline{d}$) and (2) density (ρ) multiplied by average dimension ($\rho\overline{d}$) (Fig. 4). Both maps show a N-S dispersal axis, and as expected, average block dimension diminishes with distance from the Novarupta vent. On the map of average dimension ($\overline{d}$), the 100 cm isopleth shows much less N-S elongation than the 200 cm, 50 cm, or 25 cm isopleths. This concentric shape occurs because no blocks ≥100 cm extend directly south of the vent beyond the slope separating the ignimbrite valley floor and the northern flanks of Trident. On the map that considers block size and density ($\rho\overline{d}$) (method by Parfitt and Wilson,

1999), spurs to the NE and the SE are defined by blocks 200–400 g/cm². We also examined the distribution of block lithologies (Fig. 5). Higher-density blocks, i.e., dense dacites, are slightly concentrated to the south, and low-density blocks, i.e., pumiceous dacites, are concentrated to the north, but generally the lithologies are dispersed evenly around the Novarupta dome.

Interpretation

Whereas the isopleths define boundaries beyond which certain sized blocks are not found, the size distribution of adjacent blocks is fairly random. For example, south of the current dome, a 74 cm dense dacite block sits only 260 m from a 27 cm dense dacite block and 770 m from a 25 cm pumiceous block (Figs. 4 and 5). Also, blocks of approximately the same size but of different lithology, and therefore
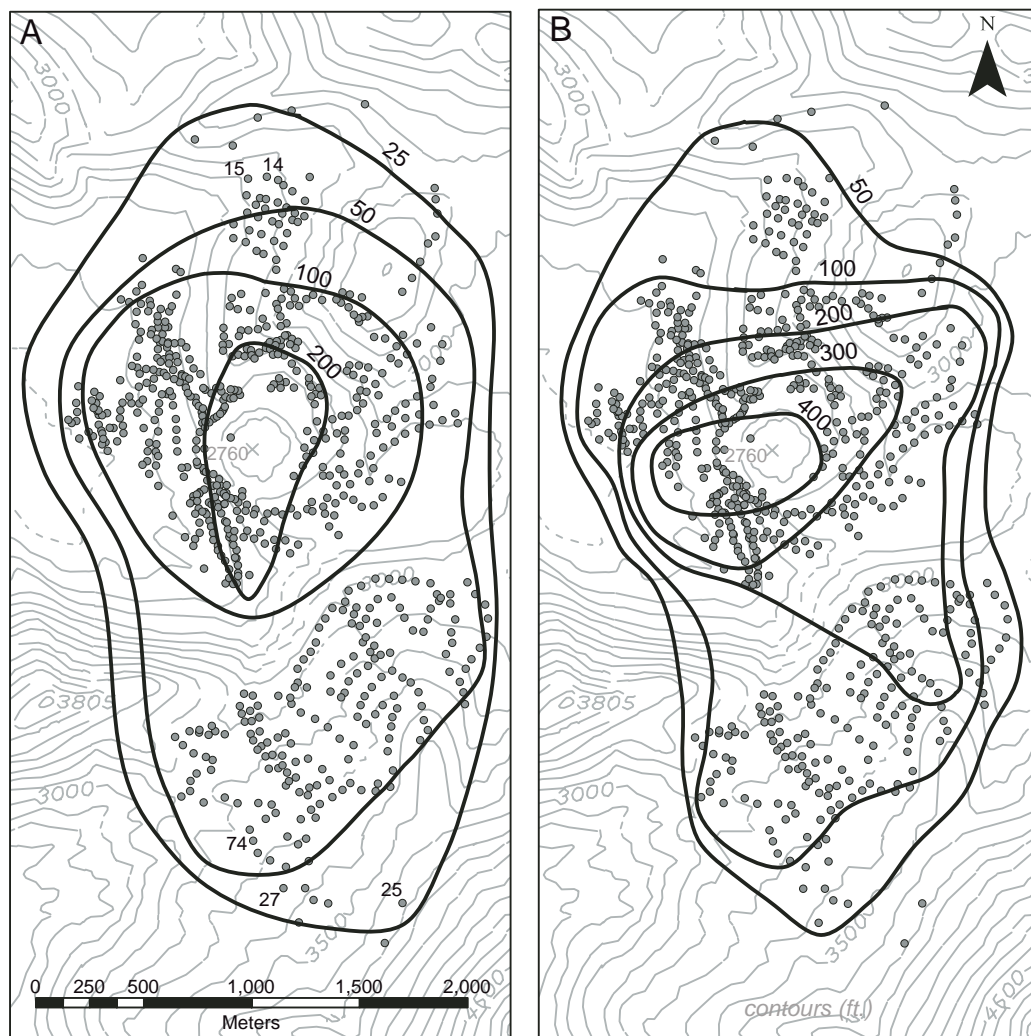

Figure 4. Distribution of block size by (A) average dimension (cm) and (B) average dimension times density (g/cm²). On both maps, isopleths enclose the current dome and define a N-S dispersal axis, but when density is considered (B), NE and SE spurs are defined. Numbered blocks are referred to in the text.

different density, traveled nearly equivalent distances, e.g., north of the current dome, a 14 cm dense dacite is adjacent to a 15 cm pumice at 1245 m. Given momentum constraints, higher-density material should have traveled farther than lower-density material of the same size. One explanation for these dispersal discrepancies might include multiple explosions during the Vulcanian phase. The distribution of lithologies in the dome prior to disruption in the vent might also have influenced the dispersal pattern, but this distribution is indiscernible based on the pattern of blocks. Other factors (atmospheric conditions, ejection angles, block shape, etc.) would also certainly affect the final distribution of block size and lithology.

Figure 5. Distribution of block lithologies. The average dimension (cm) for five blocks referred to in the text is also shown.

Block Componentry and Morphology

Data

By number, pumiceous dacites account for the largest percentage of the 200 counted blocks (Table 1). Grouping blocks by vesicularity, massive and flow-banded pumiceous blocks comprise 53.5% and massive and flow-banded dense dacites 24.5%. The remainder is mostly material of intermediate density (flow-banded mixed, lightly welded breccia, and moderately welded breccia). If the volume of each block is approximated as the product of the three principal dimensions, both study sites are volumetrically dominated by breccias and pumiceous material. While roughly half of the 200 blocks are pumiceous dacites, they make up approximately one-third of the volume of the ejecta in the studied areas. Collectively, breccias represent nearly double the material volumetrically (42%) as they do by point count (21%). Because pumiceous blocks are more likely to be broken, the correction to inferred dimension of broken blocks further reduces the relative abundance of pumiceous material.

Of the 690 mapped blocks, and excluding the 200 in the components areas, the majority of pumiceous dacites (>60%) broke into pieces upon impact, whereas the majority of breccias and dense dacites remained intact (Table 2). Not only did a majority of pumices break, but they broke into the most pieces. In fact, 60% of blocks broken into ≥6 pieces were pumiceous dacites. However, because pumiceous dacites are the most abundant lithology by count, a significant number did remain in one piece.

All lithologies contain some blocks with bread-crust exteriors; of the 690 blocks, 152 were bread-crusted. By lithology, ~30% of pumiceous dacites and ~20% of dense dacites showed bread-crust textures, whereas over 50% of flow-banded blocks were bread-crusted (Table 2). Only ~5% of breccias, including the nonjuvenile vitrophyres, remained at high enough temperatures to create bread-crust exteriors.

Interpretation

The Episode IV ejecta contain a wider range of juvenile material than seen in the Plinian falls of episodes I through III and indeed in any deposit of a Plinian eruption. While compositionally the blocks are similar to the dacites of episodes II and III, the textural diversity of the deposit suggests an original eruption style
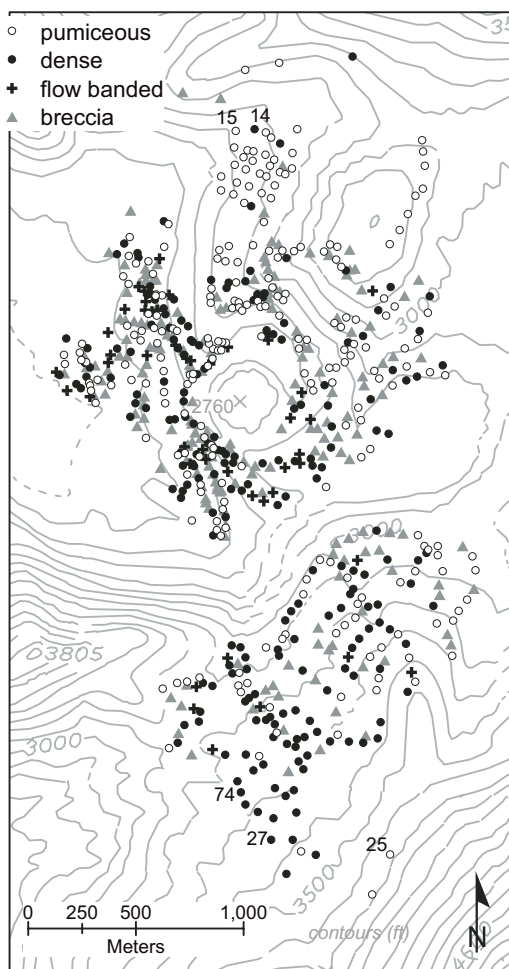
TABLE 1. RELATIVE ABUNDANCE OF LITHOLOGICAL GROUPS IN INDIVIDUAL COMPONENTRY AREAS

	Rectangle 1 (%)			Rectangle 2 (%)			Combined (%)		
	$D1*D2*D3$	$(avgD)^3$	count	$D1*D2*D3$	$(avgD)^3$	count	$D1*D2*D3$	$(avgD)^3$	count
Breccia dw	14.6	19.3	11.9	11.1	13.7	9.1	13.2	16.9	10.5
Breccia lw	1.6	2.1	3.0	4.1	4.6	3.0	2.6	3.2	3.0
Breccia mw	20.5	28.5	6.9	33.4	39.4	7.1	25.9	33.2	7.0
Dense	3.2	4.0	20.8	11.2	14.0	18.2	6.5	8.3	19.5
Fb dense	1.7	2.3	5.9	2.1	2.3	4.0	1.8	2.3	5.0
Fb mixed	0.1	0.2	1.0	1.3	1.3	2.0	0.6	0.7	1.5
Fb pums	27.4	28.3	9.9	5.0	6.2	10.1	18.2	18.9	10.0
Pumiceous	30.9	15.2	40.6	31.8	18.4	46.5	31.3	16.5	43.5

Note: dw—densely welded; lw—lightly welded; mw—moderately welded; fb—flow banded.

TABLE 2. CHARACTERISTICS OF EIGHT LITHOLOGICAL GROUPS

Lithology	Min density[†] (kg/m³)	Mean density (kg/m³)	Max density[†] (kg/m³)	Bread crust bc (%)	Bread crust lith (%)	Percentage of pieces Number of broken pieces 1	2–5	6–10	11–20	20	Percentage of lithology Number of broken pieces 1	2–5	6–10	11–20	20	Total (%)
Breccia dw	1870	2180	2400	3	4	23	15	5	5	0	73	19	5	3	0	100
Breccia lw	1080	1170	1260	0	0	3	1	0	0	0	90	10	0	0	0	100
Breccia mw	1370	2080	1720	3	7	9	15	8	5	0	47	33	15	5	0	100
Dense	1940	2390	2650	28	21	36	35	17	13	0	62	24	11	3	0	100
Fb dense	2190[‡]	2190[‡]	2190[‡]	6	41	3	1	4	5	0	55	9	23	14	0	100
Fb mixed	1290	1470	1740	3	83	1	0	2	2	0	50	0	33	17	0	100
Fb pums	730	1120	1560	7	65	0	2	7	9	0	0	18	53	29	0	100
Pumiceous	310	860	1250	49	31	25	30	57	60	100	37	18	30	14	2	100
Total (%)						100	100	100	100	100						

Note: dw—densely welded; lw—lightly welded; mw—moderately welded; fb—flow banded.
[†]Average of three minimum/maximum density blocks.
[‡]Only one of the collected samples was flow-banded (fb) dense.

much closer to dome emplacement and disruption. The range of block lithologies is matched by that seen in other silicic domes, e.g., the finely vesicular pumice, obsidian, coarsely vesicular pumice, and dense lava categories described by Fink and Anderson (2000). The distribution of these textures within a dome is complex (Fink and Manley, 1987), but most domes contain two distinct textural end members with >50% and <30% vesicles that match the pumiceous and dense dacites of the 1912 block bed.

The high degree of breakage apparent in all block lithologies, as well as the fan-shaped dispersal of the blocks broken into ≥10 pieces, is consistent with emplacement along ballistic trajectories. Widespread bread-crust textures indicate high temperatures of the ejected material and ongoing vesiculation, even after fragmentation, and also support the origin of the block bed as a hot, dacite dome or plug destroyed by Vulcanian eruption(s).

VESICULARITY OF JUVENILE MATERIAL

Techniques

To study the processes of degassing and vesiculation occurring in the conduit at Novarupta, we determined the bulk density of the samples (after Houghton and Wilson, 1989), and the data were used to select representative clasts for textural study in thin section. Heterogeneity in vesicle size and shape in a single thin section necessitates several strategies for textural analysis. Following Adams (2005), images at different magnifications were captured and analyzed, and vesicle size data were combined in order to completely characterize the size distribution of the vesicles. Vesicle areas were binned by size and converted to area (N_A) and volume (N_V) number densities following the method of Sahagian and Proussevitch (1998). Number densities refer to the number of vesicles within a certain size interval per unit area or volume. The cumulative number density (N_{Vtotal}), referenced to the matrix of the clast, i.e., total clast volume less the phenocrysts, was determined by summing the number density for each bin size (N_V) and reflects the rate and duration of nucleation of vesicles during the rise of a parcel of magma. Cumulative number densities referenced to the melt volume (N^m_{Vtotal}) have also been determined to allow for the misleading effect of the vesicle population itself on the number density (Klug et al., 2002).

Density and Bulk Vesicularity Data

Densities measured for the juvenile pumiceous and dense dacite blocks reflect a wide range of vesicularities and textures. The densities of the pumiceous blocks range between 310 and 1250 kg/m³ (Table 2), and the modal density of this subpopulation (900 kg/m³) corresponds well to the modes of the pumices deposited during the close of the Plinian activity (900–1000 kg/m³) (Fig. 6). Not surprisingly, the measured densities for the dense blocks are much higher; the majority ranges between 1940 and 2650 kg/m³. Out of the 229 pumiceous and dense dacite blocks used to measure density, only three had densities between 1530 and 1690 kg/m³. With the exception of these few transitional pieces, the pumiceous and dense dacites show no overlap in density values; a gap between 1250 and 1940 kg/m³ clearly defines the two groups.

The surface of the rhyolitic Novarupta dome, which, based on the first eyewitness accounts, has occupied the vent for a minimum of 88 yr, was also sampled, and densities were likewise determined. Measurements for this stable, long-lived dome lie almost perfectly in the gap seen in the density data for the block bed dacites (1300–2170 kg/m³) (Fig. 6).

Qualitative Observations of Vesicularity

High- (1060 kg/m³), modal- (840 kg/m³), and low-density (310 kg/m³) specimens from the sample of pumiceous dacites (HP, MP, and LP, respectively) were selected for image collection and analysis. A transitional (T) block (1690 kg/m³) between the pumiceous and dense dacites and two low-density dense dacites (D1 and D2, respectively) (2040 and 2240 kg/m³) were also selected to examine the shift between pumiceous and dense juvenile material. Specimens with densities of 1490, 1740, and 1970 kg/m³ taken from Episode V dome (R1, R2, and R3, respectively) were also analyzed (Fig. 6).

Microscopic textures in the dacite pumiceous blocks of the Episode IV dome show a progression in vesicle sizes and wall thicknesses with changing density (Fig. 7). Images of LP are comparable to pumices typical of the last phase of Plinian Episode III (Adams, 2005). Internal heterogeneity, i.e., regions where small bubbles are concentrated adjacent to regions rich in medium-coarse bubbles, characterizes LP. Heterogeneity decreases with increasing density; the distribution of a range of vesicle sizes and wall thicknesses is fairly

uniform in HP. A significant population of 2–5 μm walls is visible in LP, and while still present, their occurrence greatly diminishes in MP, which is clearly dominated by 10–15 μm walls. Thin walls are absent in HP; observed walls are consistently >25 μm thick. In all three pumiceous blocks, small bubbles are mostly associated with thicker glass walls and appear either spherical or with pinched ends. Banding is absent in MP and HP. However, bands of 0.5–1 mm width that include stretched mid-sized vesicles separated by thin glass walls, as well as thicker walls with small, pinched vesicles, sweep through the images of LP.

While indicators of bubble coalescence are abundant throughout the pumiceous dacite, the variety of features decreases with increasing density (Fig. 7). Smaller bubbles expanding into larger ones are preserved only in LP. Wrinkling of thin bubble walls separating medium-to-coarse bubbles and incomplete retraction of glass films following rupture clearly occur in both LP and MP. Thin, linear glass films separating two bubbles with approximately equal internal pressure are also seen in both LP and MP images. The above-mentioned features are almost completely absent from HP, and the bubbles are separated by wide areas of bubble-free glass. However, most of the bubbles have an amoeboid shape, suggesting an earlier history of bubble coalescence. If walls are unable to relax and regain sphericity after two or more bubbles combine, the resulting vesicle would have a complex shape, as seen in all three pumices.

Block T, representing the few blocks with measured densities between the pumiceous and dense dacites (1500–1700 kg/m³), shows alternating domains distinguishable by coarse vesicles. One type of domain has a population of millimeter-sized vesicles, whereas the largest bubbles in adjacent areas are only ~25 μm in diameter (Fig. 8A). In two-dimensional view, the domains appear to define finely spaced bands; however, in three dimensions, the geometry of the domains is more irregular. Some thin (2–5 μm) and intermediate (10–15 μm) walls are seen in the coarse-vesicle domain, but thick walls (>25 μm) clearly dominate when the coarse vesicles are not present. Amoeboid bubble shapes throughout block T indicate that coalescence played a significant role in the vesiculation history, but the loss of concavity and overall smoothness of the bubble outline, as well as a pinched appearance, describes textures created by collapse.

The progression of changing textures with increasing density of the pumiceous blocks is continued in the bubble populations of the dense dacites (≥1690 kg/m³). Coarse vesicles (~750 μm) remain in D1 (Fig. 8B), but bubble shapes are extremely irregular regardless of size, and the distribution of vesicles is largely heterogeneous. While foliation is not present, vesicles over ~500 × 500 μm areas have a stretched or flattened appearance. The contrasts between D2 and the pumiceous dacites (LP, MP, and HP) are even more severe. Voids are sparse, have irregular outlines, and show no clear association with phenocrysts (Fig. 8C). Microfractures are also increasingly pervasive in the higher-density blocks throughout the glass and crystals.

The most striking feature of the rhyolite Episode V dome specimens is foliation of the vesicles (Fig. 9). Vesicles of all sizes are elongated in the same direction; however, the vesicles themselves are not segregated into bands. As in the Episode IV dacites, vesicle size decreases and glass walls thicken with increasing density (from R1 to R3). Also, bubbles can increasingly be described as pinched or even angular in the denser rhyolite Episode V specimens, and microfractures become extensive.
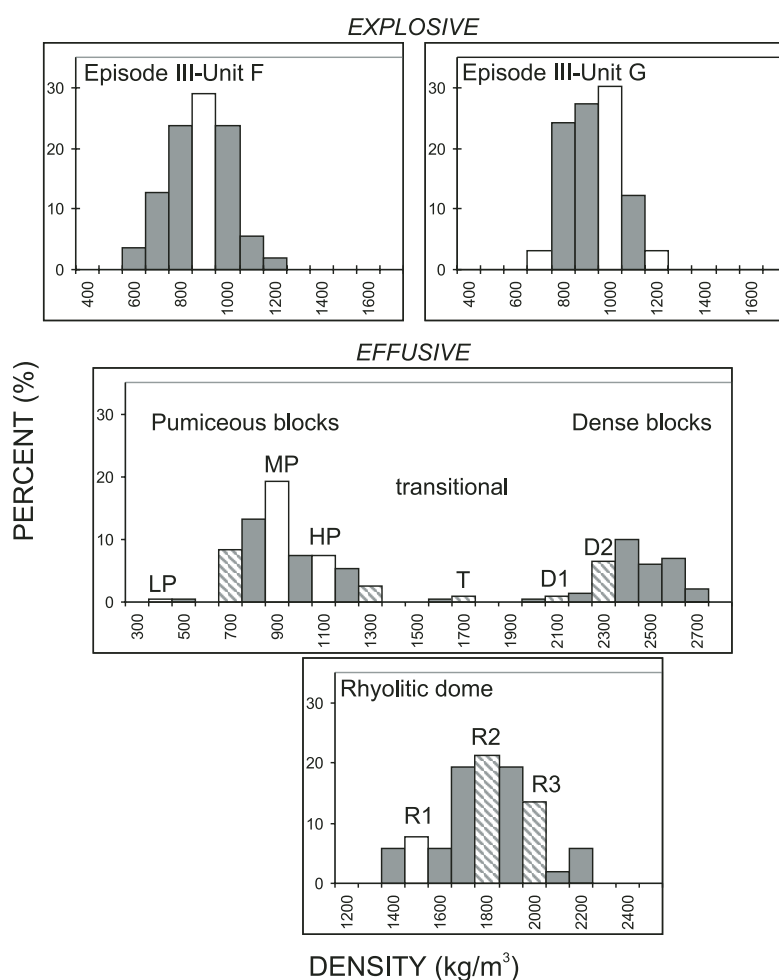

Figure 6. Density distributions measured in samples from Plinian Episode III, the block bed, and the rhyolitic Episode V dome. Densities highlighted in white correspond to individual clasts selected for image analysis; stripes indicate clasts in which images were collected but not quantified. LP, MP, and HP are low- (310 kg/m³), modal- (840 kg/m³), and high-density (1060 kg/m³) pumiceous blocks; T is transitional between pumiceous and dense (1690 kg/m³); D1 and D2 have measured densities of 2040 kg/m³ and 2240 kg/m³; R1, R2, and R3 from the Episode V dome have increasing densities of 1490 kg/m³, 1740 kg/m³, and 1970 kg/m³, respectively.
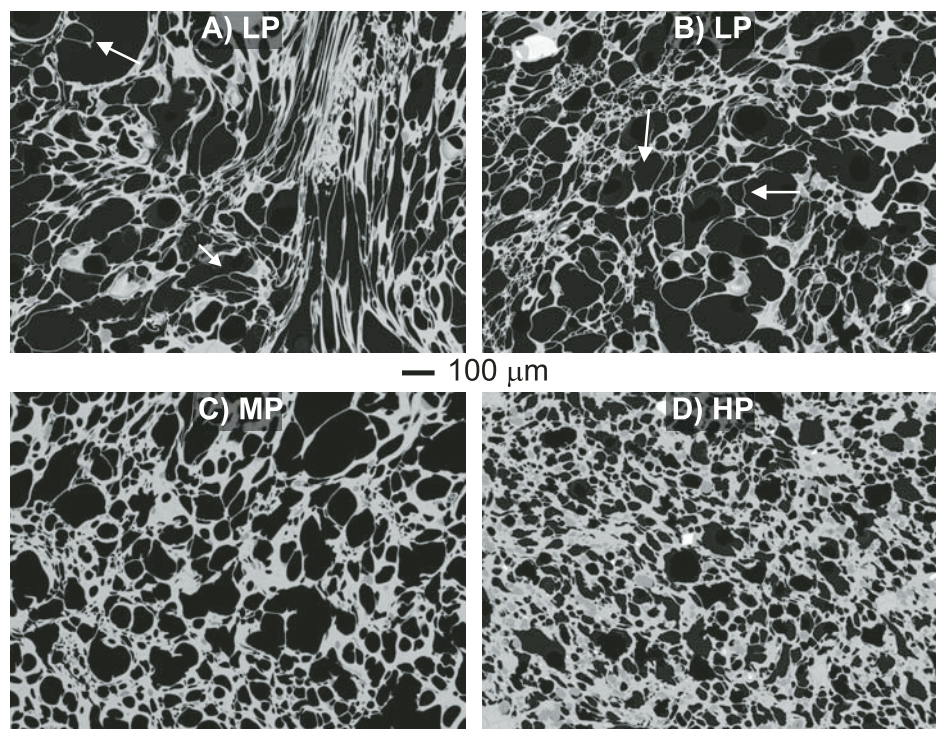
Figure 7. Backscattered-electron (BSE) images at the same scale for low- (A and B), modal- (C), and high-density (D) pumiceous blocks (LP, MP, and HP, respectively). Arrows point to coalescence features, such as very thin bubble walls, wrinkled walls, and smaller bubbles expanding into larger bubbles.
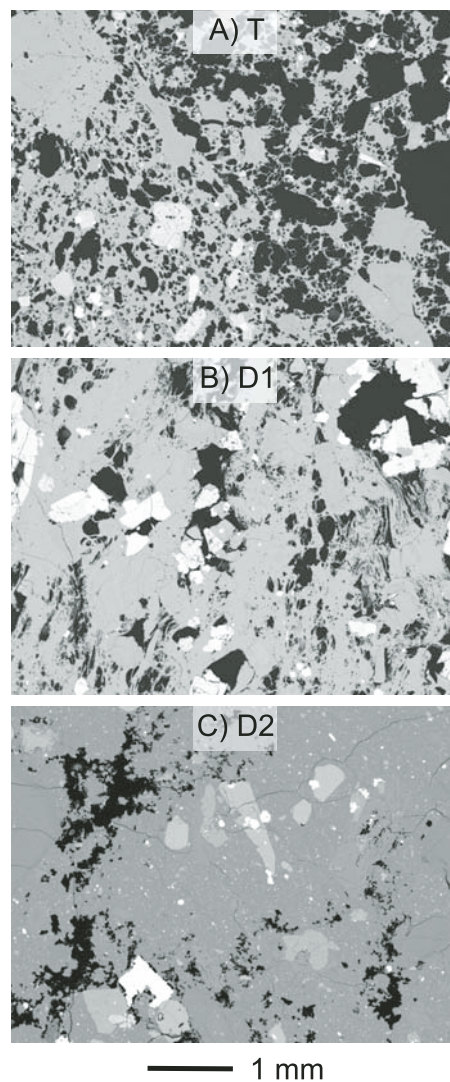

Figure 8. Backscattered-electron (BSE) images of transitional (A) and dense (B, C) dacites. Note the banded nature of the transitional dacite in A, with domains rich (top right) and poor (bottom left) in coarse vesicles.

Quantitative Observations of Vesicularity

Bubble nucleation, growth, coalescence, and collapse are all intimately related to magma ascent in the conduit, and vesicle volume distributions (VVDs) can be used to assess the contributions of these different vesiculation processes, e.g., a dominance of bubble coalescence will generally produce bimodal populations visible on histograms of volume fractions versus bubble diameter (Orsi et al., 1992; Klug and Cashman, 1994, 1996; Klug et al., 2002). On such plots, the vesicle populations from the pumiceous blocks LP, MP, and HP are unimodal like those of the Plinian pumices of Episode III (Adams, 2005). Coalescence of bubbles is responsible for a tail that characterizes all of the distributions and extends to 2–3 mm bubble sizes (Fig. 10). With increasing density (decreasing vesicularity), the size mode for the bubbles shifts from 125 μm (LP) to 50 μm (HP). The data can also be plotted as cumulative volume fraction versus diameter size, and the median vesicle sizes can be determined at the intersection of the curves with the fiftieth percentile. For the pumiceous blocks, the median sizes of LP and MP are closer in value to each other and larger compared to HP (Table 3). The timing and duration of bubble nucleation and collapse is also recorded in the cumulative number densities (N_{Vtotal} and N^m_{Vtotal}). The high-density HP has the smallest N_{Vtotal} and N^m_{Vtotal} values of the dacite pumices (Table 3).

The complex-shaped voids in the thin sections of the denser dacites (≥ 1690 kg/m^3), i.e., T, D1, and D2, as well as the intermediate- (1740 kg/m^3) and high-density (1970 kg/m^3) Episode V dome samples (R2 and R3), cannot be quantified by the previously described methods; thus, VVDs and cumulative number densities have not been determined for these samples. Statistical problems arise from too few bubbles per clast, and the irregularity in shape makes sphere-based conversions to volume invalid.

Interpretation

All quantitative data from the pumiceous Episode IV blocks point to (1) an extended and diverse vesiculation history, and (2) a continuation of the changes first observed at the end of Episode III (Adams, 2005). Early exponential nucleation and growth was overprinted by bubble coalescence as melt advanced through the conduit and then, for some portions of the magma, by the onset of bubble collapse. Qualitatively, bubble coalescence is apparent throughout the pumiceous dacites, but quantitatively, its influence on the bubble size distribution diminishes in the denser blocks as bubble collapse becomes a dominant process. Not only are coalescence features less prominent in
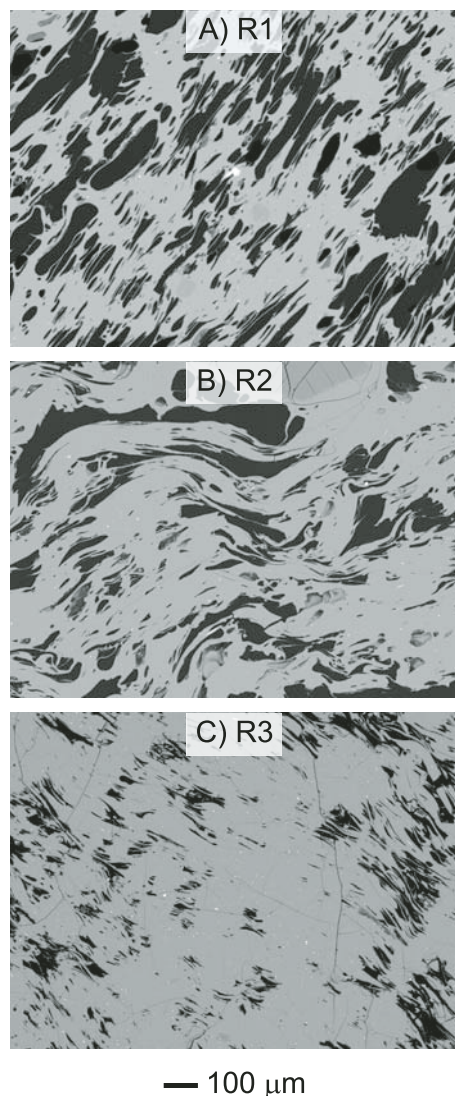
— 100 μm

Figure 9. Backscattered-electron (BSE) images of rhyolitic Episode V dome. Notice the increase in microfractures as density increases.

Figure 10. Distributions of vesicle volume for low- (310 kg/m³), modal- (840 kg/m³), high-density (1060 kg/m³) pumiceous blocks, and Episode V dome (LP, MP, HP, and R1, respectively). (Top) Histograms showing the distribution of volume fraction against vesicle size. (Bottom) Cumulative volume percent plot; intersection of 50th percentile with curves gives median vesicle sizes.

HP compared to MP and LP, but the glass walls are noticeably thicker, the distribution of sizes is less heterogeneous, and the dominant bubble size is smaller (Fig. 7), all of which is consistent with collapse of bubbles. The median bubble size is more than 20 μm smaller for HP compared to MP and LP (Fig. 10; Table 3). Coalescence drives bubble size distributions toward larger sizes (Cashman and Mangan, 1994), and while coalescence features are also evident qualitatively, collapse has had a stronger effect on the size distribution in HP. The significance of collapse in HP is also reflected by the lower cumulative number density and the smaller
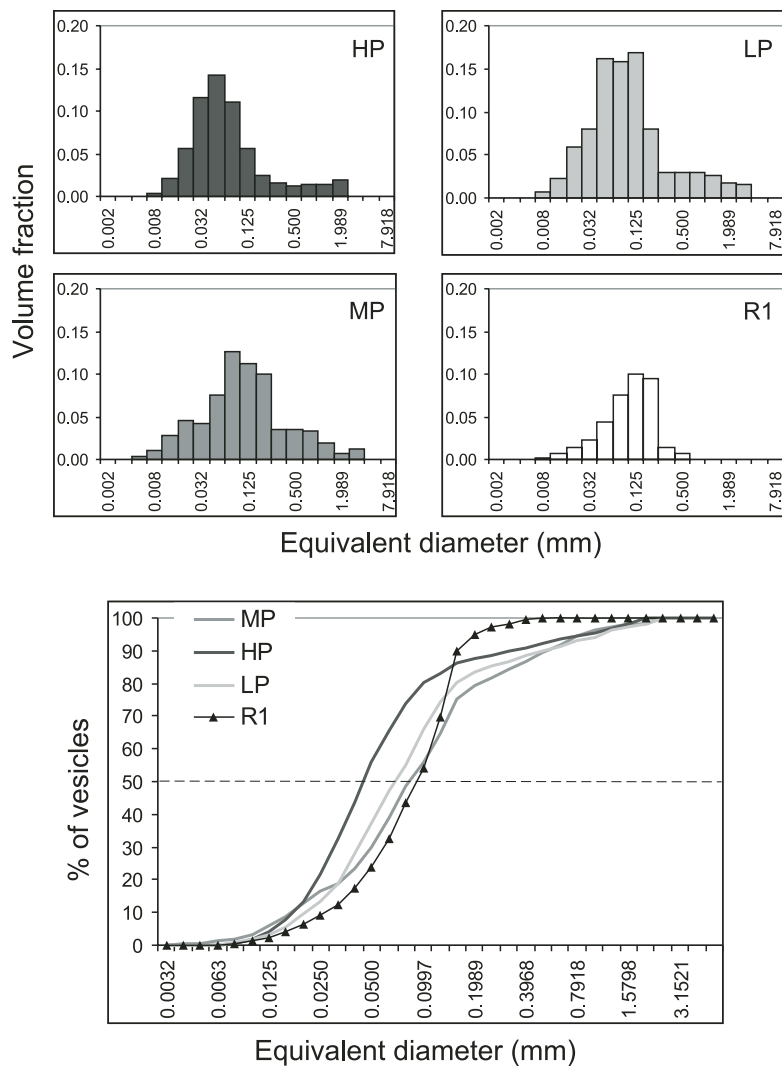
modal value on the VVD histogram. Collapse would be expected to reduce the total number of bubbles and the overall bubble size. HP has the smallest N^m_{Vtotal}, and despite coalescence-created coarse tails, peak values decrease with increasing density on VVD histograms (Fig. 10; Table 3). We suggest that this trend reflects contrasts in residence time in the dome and shallow conduit, as discussed in detail in the following.

The density gap between pumiceous and dense dacite is matched by striking dissimilarities between the bubble populations. However, the dense dacites appear to have similar

but more extended vesiculation histories than their pumiceous analogs. Low vesicularity, observably low bubble number densities, and the irregular distribution of clusters of pinched and deformed vesicles in areas of vesicle-free glass suggest that the dense dacites are the end products of outgassing and bubble collapse. We suggest that the apparent gap between dense and pumiceous dacite of Episode IV is strong, indirect evidence that once bubble collapse is initiated by the onset of permeability, it is a catastrophic process that advances rapidly to completion and generates an outgassed and rheologically stiffened melt phase.

TABLE 3. PARAMETERS FOR REPRESENTATIVE SAMPLES

	Block	Density (kg/m³)	Crystallinity (%)	Ves. (%)	$N_{A\ total}$ (cm⁻²)	$N_{V\ total}$ (cm⁻³)	$N^m_{V\ total}$ (cm⁻³)	n no./cm⁻³/cm	Size range (µm)	Median (µm)	Number included
	LP	310	16	87.3	1.5×10^6	1.2×10^8	4.9×10^8	5.1×10^{11}	8–2504	68	2558
Pumiceous		670		72.5							
Dacite	MP	840	19	65.8	2.3×10^6	3.4×10^8	8.10×10^8	2.8×10^{12}	4–2504	84	1774
Blocks	HP	1060	24	56.6	1.5×10^6	1.1×10^8	2.6×10^8	4.2×10^{11}	8–1989	45	2780
		1220		50.1							
Transitional	T	1690	98†	31.2							
Dense dacite	D1	2040	33	16.7							
Blocks	D2	2240	100†	8.6							
Episode V	R1	1490	3	38.1	8.6×10^5	5.9×10^7	1.10×10^8	2.4×10^{11}	8–630	92	1695
Rhyolite	R2	1740	6	27.3							
Dome	R3	1970	5	17.7							

Note: Blocks were chosen for vesicle quantification to span the densities measured per lithology. Vesicle shapes in higher-density clasts (>1600 kg/m³) prevent vesicle volume calculations. DRE (dense rock equivalent) values of 2350 and 2450 kg/m³ were used to calculate vesicularities for rhyolites and dacites, respectively. $N_{A\ total}$ is areal number density of vesicles; $N_{V\ total}$ is volumetric number density of vesicles referenced to the whole clast; $N^m_{V\ total}$ is volumetric number density of vesicles referenced to the melt only; n is population number density.
†An approximate value; microlites are abundant.

DYNAMICS OF BLOCK BED EMPLACEMENT

Methodology and Model Parameters

Based on our field work, we infer that the Episode IV dome/plug capped the Novarupta vent during a period of passive lava effusion and at some point underwent explosive disaggregation to produce the observed block field. This most likely took place as one or more discrete, transient explosions driven by the sudden release of pressurized gas trapped beneath the cap rock. To better understand the mechanism of disruption and ejection of the Episode IV dome, we have modeled the dynamics of explosive dispersal of ballistic blocks.

Previous work on transient (Vulcanian-style) volcanic explosions has recognized that the distance traveled by a ballistic block can be related (via a trajectory equation) to its ejection velocity. The velocity, in turn, can be related to the amount and degree of pressurization of the gas driving the explosion via an equation of motion (Minakami, 1950; Gorshkov, 1959; Decker and Hadikusumo, 1961; Fudali and Melson, 1972; Melson and Saenz, 1973; Steinberg, 1977; Steinberg and Babenko, 1978; Self et al., 1979, 1980; Wilson, 1980; Fagents and Wilson, 1993). Early work neglected or mistreated atmospheric drag interactions with the ejected blocks, leading to inaccurate velocity predictions. Furthermore, use of inappropriate equations of motion or velocity overestimates led to unrealistically high explosion pressures. In explicitly treating

the dynamics of gas expansion (Wilson, 1980) and ejection of blocks into an atmosphere set in motion by the blast (Fagents and Wilson, 1993), it has been shown that block fields at several volcanoes could plausibly be explained with only modest gas pressures (<20 MPa) and eruption velocities of a few tens to a few hundred meters per second. The required gas mass fractions typically exceed magma volatile contents, implying a segregation and accumulation of gases in the shallow conduit or a role for external water (Fagents and Wilson, 1993).

In modeling the Episode IV dome ejection, we adopted the numerical method of Fagents and Wilson (1993), which treats the dynamics of transient explosions in detail. This model takes as its starting point an amount of gas held at pressure that, following sudden decompression, displaces and accelerates a dense slug of cap rock plus a mass of atmospheric gas overlying the explosion site. The Fagents and Wilson (1993) model integrates the equation of motion of the solid and gaseous ejecta to yield the ejection velocity. This velocity is then used as the starting condition to compute the ballistic trajectories and landing points of dome fragments, subject to the aerodynamic forces imposed by the motions induced in the volcanic and atmospheric gases. Our approach, therefore, was to compare the mapped locations of Novarupta blocks with model predictions for a variety of plausible initial conditions, and thus infer the ejection velocities, initial pressures, and volatile concentrations responsible for the observed distribution of ejecta. The

objective was to determine whether estimated gas quantities and pressures can plausibly produce the observed block field.

For the Novarupta Episode IV block bed, bubble collapse to form surface and near-surface dense dacite might have hindered outgassing of enclosed and still actively degassing pumiceous lava. Continued gas exsolution would then have led to a rise in gas pressure at greater depths within the dome and conduit. Initiation of an explosion would have occurred once the gas pressure exceeded that due to the overlying dome mass or when the cool outer dome material failed in a brittle manner. We employed a range of model parameters constrained by the field data.

Initial Gas Pressure

Bubble textures and bread-crust exteriors to blocks suggest that the dome was only partially solidified prior to disruption and ejection. The pre-explosion gas pressure would therefore have had to overcome a bulk lava strength consisting of the yield strength of the molten portion and the tensile strength of the solid portion. Yield strengths for high-silica rocks are typically of the order 0.1 MPa (Moore et al., 1978; Blake, 1990). An upper limit for tensile strength based on measurements of pristine samples of igneous rocks might be ~10 MPa (Touloukian et al., 1981). However, thermal stress, cooling cracks, the presence of pressurized gases, and high strain associated with high crystal contents in hot dacite dome material (Mellors et al., 1988; Sato et al., 1992) could reduce the rock strength

to much lower values. Perhaps a more important consideration is the depth from which the explosion initiated, e.g., a depth of 100 m beneath the dome surface corresponds to a hydrostatic pressure (= $\rho g z$) of ~2.5 MPa. An extreme limit is perhaps 1000 m depth (25 MPa) if fragmentation extended to deep in the conduit. Given the uncertainties in the strength of dome material, we therefore adopted a range of initial pressure of 2.5–25 MPa. Although this choice of depths was somewhat arbitrary, it allowed us to bracket the range of plausible pre-explosion pressures.

Gas Mass Fraction

The model also required a value of the mass ratio, n, of gas to solid ejecta. This is the parameter that we were interested in finding by producing model predictions consistent with the block field data. However, we also had to consider the limits imposed by the textural analyses. It is possible to derive an estimate of the minimum pre-explosion bulk gas concentration from the vesicularity of ejecta. Our initial consideration was that the explosions were driven only by magmatic gas expanding within pumiceous dacite melt but which ejected a range of block types derived from overlying capping lava. Using our data, the pumice represents ~16.6% by volume of the ejecta, and an average pumice vesicularity of 68% implies that ~11% by volume of the pre-ejection dome material was gas available to drive the eruption. This volume can be converted to gas/solid mass ratio if we know the gas density, which is a function of the confinement pressure and gas temperature. Using the 2.5–25 MPa range with a temperature of 600 °C yielded gas/solid mass values of $n = 0.002$–0.0045 (0.2–0.45 wt%). Although heterogeneities in gas concentration undoubtedly occurred within the dome rock (as evidenced by the variety of block types mapped), this bulk gas fraction (averaged over the dome volume) provided a lower bound on the gas available to drive the eruption.

Additional Parameters

We accounted for a variety of blocks ranging in size from 0.25 to 2.3 m in average diameter, having densities from 860 kg/m^3 (pumice) to 2390 kg/m^3 (dense dacite), and ejected to distances from 230 to 2200 m from the vent. Differences in the elevations of the ejection and impact sites were also considered; a block lying lower than the vent requires a lower ejection velocity than one lying at the same horizontal distance but

at the same elevation as the vent. Atmospheric conditions corresponding to the Novarupta location were incorporated into the model, and the optimum ejection angle of 45° was adopted to derive the minimum required velocities. Finally, the ejection and trajectory-tracing algorithms were run to investigate the conditions required to produce the observed block distribution.

Results

We find that blocks projected to the medial and distal portions of the block field require significant enhancement in gas abundances over that provided by the pumice alone. Typically, blocks ejected beyond ~1 km require $n > 0.015$–0.040 (>1.5–4 wt%) and ejection velocities in the range $u = 100$–200 m s^{-1} (Fig. 11). These ranges of n and u could be produced by multiple explosions, or the range in ejection distance could result from a single explosion ejecting blocks at a variety of launch angles. Some blocks, particularly the smaller, low-density pumice clasts, require gas/solid mass ratios and ejection velocities that we deem to be unrealistically high ($n > 10$–20 wt%, $u > 400$ m s^{-1}). In these cases, a role for convective support and/or wind dispersal is probably implied for these distances to be attained. Alternatively, some of these blocks may have broken in flight. Larger blocks falling within 1 km of the vent require much lower ejection velocities (45–75 m s^{-1}) and gas/solid mass ratios (0.4–1 wt%) (Fig. 11), much closer to those provided by pumice-derived gas alone (0.2–0.45 wt%).

In exploring the sensitivity of model results, we find that for gas mass fractions <0.05 (5 wt%), the predicted velocities and ejection distances are relatively insensitive to the range of initial gas pressure investigated (and hence depth of origin of explosion) (Fagents and Wilson, 1995). A more important factor is the angle of ejection of the blocks, taken here as the optimum, 45°. Thus, the results shown in Figure 11 are minimum values; the proximal blocks could just as plausibly have been ejected in more intense, gas-rich explosions but at greater launch angles to follow steeper trajectories and still land close to the vent. While the results shown in Figure 11 are subject to the validity of our assumptions and the constraints on model parameters, our principal conclusion remains valid. Significantly higher gas abundances than can be provided by the pumice alone are implied for at least some of the 1912 explosions.

DISCUSSION AND CONCLUSIONS

Magma Ascent and Degassing

Textures in the dacitic pyroclasts of Episode III and the Episode IV block bed reflect the changing degassing conditions of a system shifting between explosive to effusive eruption styles via an interval of transient growth of an unstable and texturally heterogeneous lava dome. Reduced mass flux and ascent velocity by the end of Episode III was accompanied by a partial switch between closed- and open-system degassing, which preferentially affected melt ascending along the margins of the conduit (Adams, 2005). Melt along the conduit axis continued to ascend rapidly and to nucleate and grow vesicles at shallow depths, while rheological stiffening accompanying degassing caused other adjacent but more stagnant melt undergoing bubble collapse to line the conduit margins. Continued lining effectively reduced the radius of the conduit. The outgassed material eventually blocked the shallowest levels of the conduit, and Plinian activity stopped altogether. However, volatile-rich material that remained deeper in the conduit continued to rise, driving the overlying outgassed, but still fluid, melt through the conduit to form a dome or plug.

We thus picture a combination of coeval open- and closed-system degassing occurring at similar levels in the conduit during an essentially unstable transition period (between stable Plinian eruption in Episode III and stable dome growth in Episode V). The pumiceous component of the assemblage of blocks represents the initially deeper melt characterized by an ascent history similar to the dacite of Episode III, i.e., it experienced closed-system and disequilibrium degassing. Ascent and vesiculation of this deeper magma drove dome/plug extrusion, and it involved the relatively dense, outgassed magma in its ascent. Fingers of relatively hot, vesiculating magma intruded the cooler, denser, and largely outgassed material (Fig. 12), so that the dome/plug was characterized by domains of dense and pumiceous dacite (Fig. 13). The bimodal distribution of textures, i.e., dense versus pumiceous dacite, may reflect (1) rapid onset of a short period of permeability and gas escape from melt, or (2) a time gap between the arrival of the melt forming the dense dacite at the end of Episode III and ascent of the pumiceous dacite. Westrich and Eichelberger (1994) have suggested that bubble collapse is

followed quickly by a decrease in permeability and the system then closes to gas flow; the time interval of bubble collapse is, a priori, short. At Novarupta, loss of permeability through catastrophic bubble collapse in portions of the ascending melt might have led to a release of exsolved volatiles and disruption of the dome through Vulcanian explosion(s). Perhaps Episode IV was analogous to historic eruptions of silicic domes that exhibit cyclic activity of extrusion and disruption caused by reduced permeability and subsequently increased pressurization, e.g., Lascar Volcano, Chile, and Soufrière Hills Volcano, Montserrat, British West Indies (Matthews et al., 1997; Voight et al., 1999). The model proposed by Matthews et al. (1997) involves extrusion of dome lava accompanied by vesiculation in the conduit and dome interior. Partial outgassing through permeable vesicular magma leads to bubble collapse and inhibition of open-system degassing. Minor explosions are related to discrete collapse events in the shallow environment, and major eruptions involve loss of permeability at greater depths. In terms of textures, the Episode IV dome fits this model for cyclic dome growth. The distribution of blocks by size does not exclude multiple explosions, but currently we can only speculate if the activity during Episode IV was cyclic in nature.

Why was the Episode IV dome unstable and Episode V characterized by stable dome growth? We suggest that a greater degree of textural heterogeneity in the dacite melt affected the outcome of the Episode IV dome. Compared to lava from the stable Episode V dome, Episode IV blocks have a wider range of vesicularities and bubble sizes. While both episodes show textures implying bubble collapse, the diversity in textures within the Episode IV magma shows that portions of it were characterized by closed-system vesiculation. These portions of the dacite melt that underwent rapid disequilibrium degassing resulted in a dome that was on the verge of fragmentation and explosive eruption; modeling suggests a possible addition of external water might have triggered disruption. Conversely, the textures in the Episode V dome represent long-term and more consistent open-system degassing, which is logical if this melt was resident in parts of the shallow conduit since the close of Episode I. These textures perhaps represent a later stage of development involving extended residence in the shallow conduit and passive outgassing.
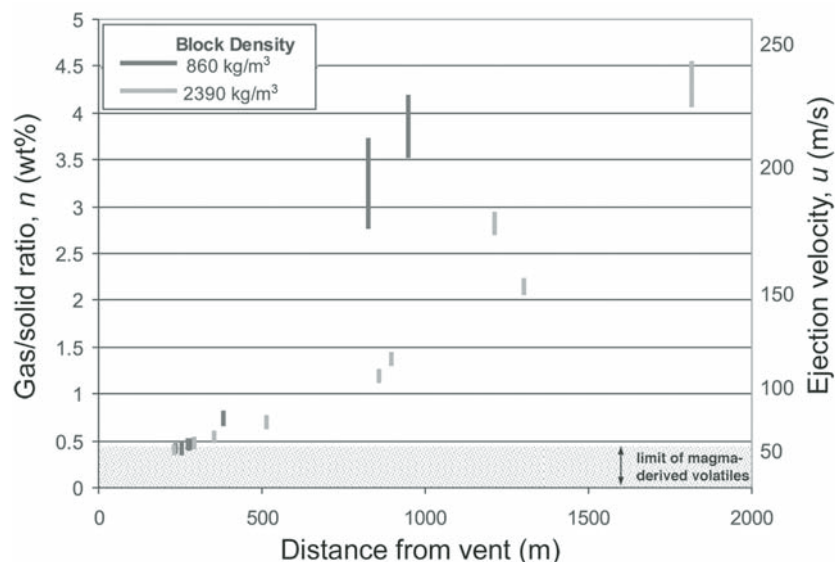

Figure 11. Model results showing relationship between relative amount of gas and velocities needed to disperse blocks of a given size and distance.
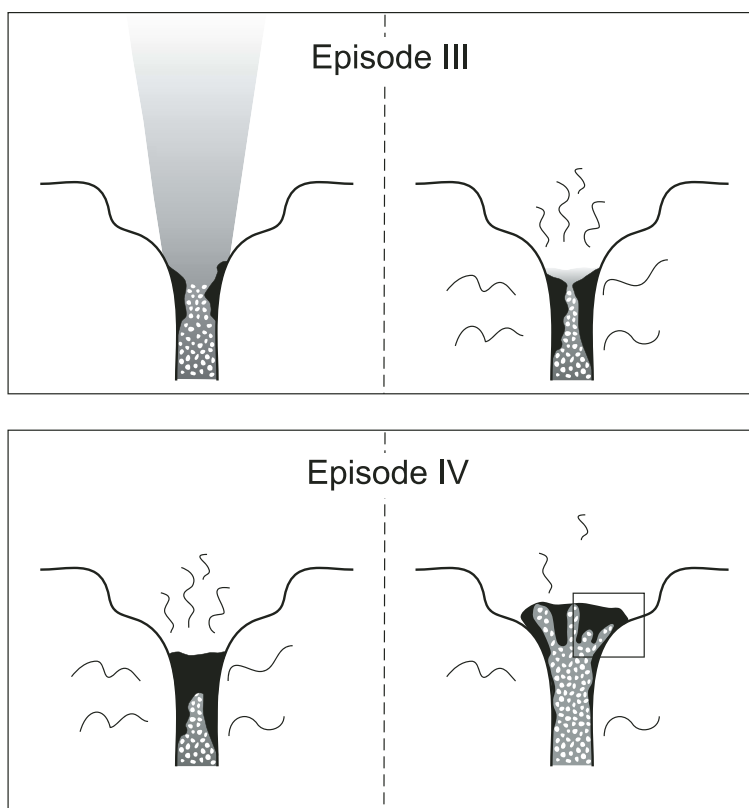

Figure 12. Cartoon illustrating shifts in eruption style and degassing during episodes III and IV. As open-system degassing intensified, magma and gas decoupled and gas escaped freely, marking the end of Plinian activity and Episode III. Degassed, dense magma accumulated on the conduit walls; the dense magma eventually capped the vent and was ultimately extruded by gas-rich dacite still ascending. Bubble collapse removed pathways for gas to escape, gas exsolution exceeded the capacity of the system to passively degas, and Vulcanian eruptions ensued. Rectangular region in last panel is enlarged in Figure 13.
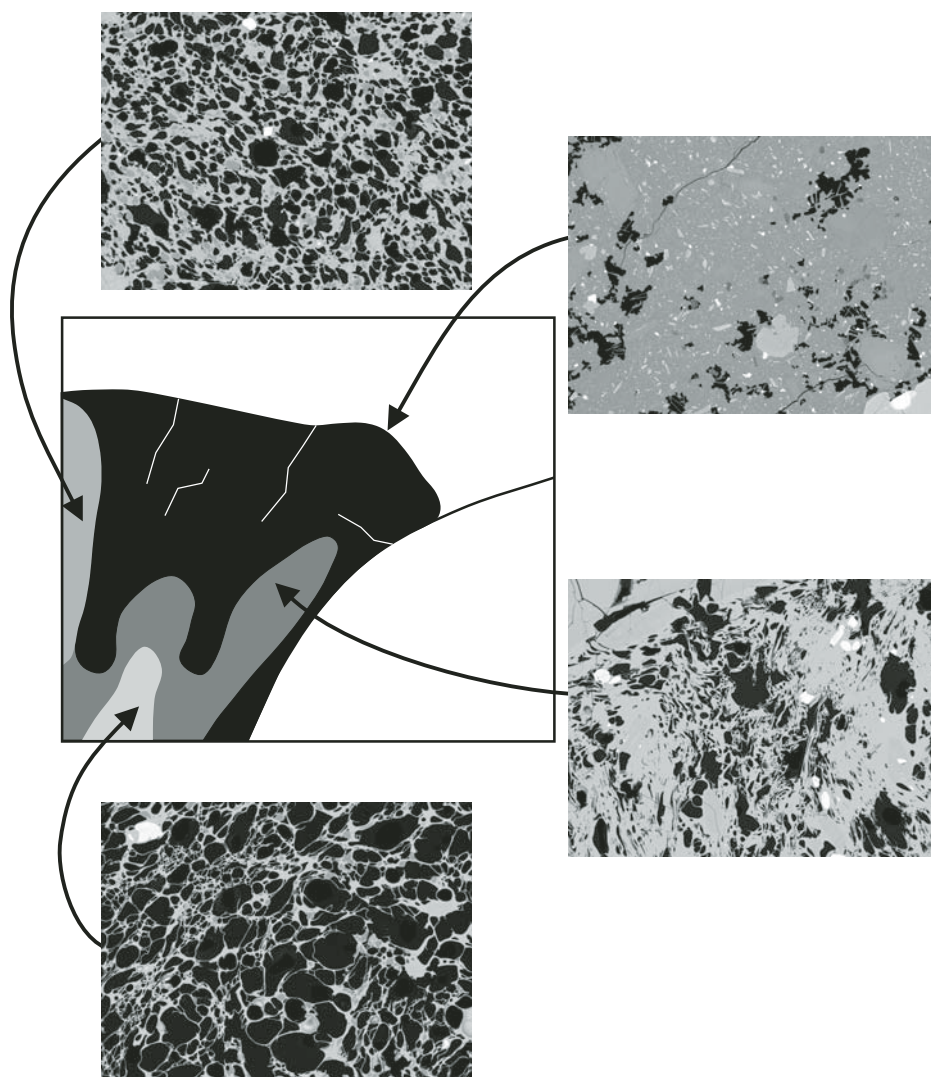
of gas, perhaps via external water, to the system. Given the cool, maritime climate of the Alaskan peninsula and the timing of the eruption, two possible precipitants may be relevant. Rainfall that occurred after the dome was largely extruded but was still relatively hot could have entered the magma through cracks and microfractures. Alternatively, while snowfall is not common from late June through August at Katmai, snow that predated the Plinian eruption on 6 June could have been trapped below the pyroclastic fall deposits that filled the crater. Both of these sources might have provided sufficient external volatiles to boost Vulcanian explosions driven predominantly by the expanding magmatic volatiles. Furthermore, the intrusion of external water to pockets of trapped gas (as previously described) might trigger fragmentation of portions of the dome and lead to ultimate destruction.

ACKNOWLEDGMENTS

REFERENCES CITED

Adams, N.K., 2005, Magma degassing during the 1912 eruption of Novarupta, Alaska: Textural analyses of pyroclasts representing changes in eruptive intensity and style [Ph.D. thesis]: Honolulu, University of Hawaii, 177 p.

Anderson, S.W., and Fink, J.H., 1989, The development and distribution of surface textures at the Mount St. Helens dome, *in* Fink, J., ed., Lava flows and domes: Emplacement Mechanisms and Hazard Implications: Berlin, Springer-Verlag, IAVCEI (International Association of Volcanology and Chemistry of the Earth's Interior) Proceedings in Volcanology, p. 25–46.

Anderson, S.W., Fink, J.H., and Rose, W.I., 1995, Mount St. Helens and Santiaguito lava domes: The effect of short-term eruption rate on surface texture and degassing processes: Journal of Volcanology and Geothermal Research, v. 69, p. 105–116, doi: 10.1016/0377-0273(95)00022-4.

Barmin, A., Melnik, O., and Sparks, R.S.J., 2002, Periodic behavior in lava dome eruptions: Earth and Planetary Science Letters, v. 199, p. 173–184, doi: 10.1016/S0012-821X(02)00557-5.

Blake, S., 1990, Viscoplastic models of lava domes, *in* Fink, J.H., ed., Lava flows and domes: Emplacement Mechanisms and Hazard Implications: Berlin, Springer-Verlag, p. 88–128.

Cashman, K.V., 1992, Groundmass crystallization of Mount St. Helens dacite, 1980–1986—A tool for interpreting shallow magmatic processes: Contributions to Mineralogy and Petrology, v. 109, p. 431–449, doi: 10.1007/BF00306547.

Cashman, K.V., and Mangan, M.T., 1994, Physical aspects of magmatic degassing, II, Constraints on vesiculation processes from textural studies of eruptive products, *in* Carroll, M.R., and Holloway, J.R., eds., Volatiles in magmas: Washington, DC, Mineralogical Society of America, p. 447–478.

Cashman, K.V., and Marsh, B.D., 1988, Crystal size distribution (CSD) in rocks and the kinetics and dynamics of crystallization, II, Makaopuhi Lava Lake: Contributions to Mineralogy and Petrology, v. 99, p. 292–305, doi: 10.1007/BF00375363.

Figure 13. Enlarged region on Figure 12. Heterogeneity in the Episode IV melt affected the outcome, i.e., disruption, compared to the stability of the Episode V dome.

Model for Dome Fragmentation

Our preferred model for fragmentation of the Episode IV dome includes rapid expansion of magmatic volatiles formerly trapped in rising pumiceous dacite. One scenario that might involve such rapid expansion and catastrophic release of gases follows the model discussed by Matthews et al. (1997). The Episode IV block textures are indicative of cyclic dome growth involving disruption after an increase in pressurization caused by reduced permeability (e.g., Matthews et al., 1997). Continuing with that scenario and again considering the heterogeneity of the Episode IV dome, pockets of volatiles escaping from the pumiceous material could be partially trapped and concentrated by domains of denser material.

A weakness, such as a fracture or gravitational collapse of part of the dome edifice, might have released this pressurized gas, which was localized within the dome complex, and triggered an explosion. Similar models have been suggested by Voight and Elsworth (2000) for dome collapse and by Ui et al. (1999) for generation of block and ash flows. In the section Dynamics of Block Bed Emplacement, we shifted our attention from textural observations and considered the amount of gas needed versus the amount available to ballistically emplace blocks characterized by the Episode IV densities, shapes, and distances traveled. In terms of gas/solid mass ratios, a second scenario can be envisioned. The high gas/solid mass ratios required for the dispersal of smaller, low-density blocks suggest an additional source

Cashman, K.V., Sturtevant, B., Papale, P., and Navon, O., 2000, Magmatic fragmentation, *in* Sigurdsson, H., ed., Encyclopedia of volcanoes: San Diego, California, Academic Press, p. 421–430.

Curtis, G.H., 1968, The stratigraphy of the ejecta of the 1912 eruption of Mount Katmai and Novarupta, Alaska: Geological Society of America Bulletin, v. 72, p. 153–210.

Decker, R.W., and Hadikusumo, D., 1961, Results of the 1960 expedition to Krakatau: Journal of Geophysical Research, v. 66, p. 3497–3511.

Eichelberger, J.C., 1995, Silicic volcanism: Ascent of viscous magmas from crustal reservoirs: Annual Review of Earth and Planetary Sciences, v. 23, p. 41–63, doi: 10.1146/annurev.ea.23.050195.000353.

Eichelberger, J.C., Carrigan, C.R., Westrich, H.R., and Price, R.H., 1986, Non-explosive silicic volcanism: Nature, v. 323, p. 598–602, doi: 10.1038/323598a0.

Fagents, S.A., and Wilson, L., 1993, Explosive volcanic eruptions, VII, The ranges of pyroclasts ejected in transient volcanic explosions: Geophysical Journal International, v. 113, p. 359–370.

Fagents, S.A., and Wilson, L., 1995, Explosive volcanism on Venus: Transient volcanic explosions as a mechanism for localized pyroclast dispersal: Journal of Geophysical Research, v. 100, p. 26,327–26,338, doi: 10.1029/95JE03202.

Fierstein, J., and Hildreth, W., 1992, The Plinian eruptions of 1912 at Novarupta, Katmai National Park, Alaska: Bulletin of Volcanology, v. 54, p. 646–684, doi: 10.1007/BF00430778.

Fink, J.H., and Anderson, S.W., 2000, Lava domes and coulees, *in* Sigurdsson, H., ed., Encyclopedia of volcanoes: San Diego, California, Academic Press, p. 307–319.

Fink, J.H., and Manley, C.R., 1987, Origin of pumiceous and glassy textures in rhyolite flows and domes, *in* Fink, J., ed., The emplacement of silicic domes and lava flows: Geological Society of America Special Paper 212, p. 77–88.

Fink, J.H., Malin, M.C., and Anderson, S.W., 1990, Intrusive and extrusive growth of the Mount St. Helens lava dome: Nature, v. 348, p. 435–437, doi: 10.1038/348435a0.

Fudali, R.F., and Melson, W.G., 1972, Ejecta velocities, magma chamber pressure and kinetic energy associated with the 1968 eruption of Arenal volcano: Bulletin of Volcanology, v. 35, p. 383–401.

Gardner, J.E., Hilton, M., and Carroll, M.R., 1999, Experimental constraints on degassing of magma: Isothermal bubble growth during continuous decompression from high pressure: Earth and Planetary Science Letters, v. 168, p. 201–218, doi: 10.1016/S0012-821X(99)00051-5.

Gorshkov, G.S., 1959, Gigantic eruption of volcano Bezymianny: Bulletin of Volcanology, v. 35, p. 77–109.

Hildreth, W., 1983, The compositionally zoned eruption of 1912 in the Valley of Ten Thousand Smokes, Katmai National Park, Alaska: Journal of Volcanology and Geothermal Research, v. 18, p. 1–56, doi: 10.1016/0377-0273(83)90003-3.

Hildreth, W., 1987, New perspectives on the eruption of 1912 in the Valley of Ten Thousand Smokes, Katmai National Park, Alaska: Bulletin of Volcanology, v. 49, p. 680–693, doi: 10.1007/BF01080359.

Hildreth, W., and Fierstein, J., 2000, Katmai volcanic cluster and the great eruption of 1912: Geological Society of America Bulletin, v. 112, p. 1594–1620, doi: 10.1130/0016-7606(2000)112<1594:KVCATG>2.0.CO;2.

Houghton, B.F., and Wilson, C.J.N., 1989, A vesicularity index for pyroclastic deposits: Bulletin of Volcanology, v. 51, p. 451–462, doi: 10.1007/BF01078811.

Houghton, B.F., Wilson, C.J.N., Fierstein, J., and Hildreth, W., 2004, Complex proximal deposition during the Plinian eruptions of 1912 at Novarupta, Alaska: Bulletin of Volcanology, v. 66, p. 95–133, doi: 10.1007/s00445-003-0297-7.

Jaupart, C., 1996, Physical models of volcanic eruptions: Chemical Geology, v. 128, p. 217–227, doi: 10.1016/0009-2541(95)00175-1.

Jaupart, C., 1998, Gas loss from magmas through conduit walls during eruption, *in* Gilbert, J.S., and Sparks, R.S.J., eds., The physics of explosive volcanic eruptions: Geological Society [London] Special Publication 145, p. 73–90.

Jaupart, C., and Allegre, C.J., 1991, Gas content, eruption rate and instabilities of eruption regime in silicic volcanoes: Earth and Planetary Science Letters, v. 102, p. 413–429, doi: 10.1016/0012-821X(91)90032-D.

Klug, C., and Cashman, K.V., 1994, Vesiculation of May 18, 1980, Mount St. Helens magma: Geology, v. 22, p. 468–472, doi: 10.1130/0091-7613(1994)022<0468:VOMMSH>2.3.CO;2.

Klug, C., and Cashman, K.V., 1996, Permeability development in vesiculating magmas: Implications for fragmentation: Bulletin of Volcanology, v. 58, p. 87–100, doi: 10.1007/s004450050128.

Klug, C., Cashman, K.V., and Bacon, C.R., 2002, Structure and physical characteristics of pumice from the climactic eruption of Mount Mazama (Crater Lake), Oregon: Bulletin of Volcanology, v. 64, p. 486–501, doi: 10.1007/s00445-002-0230-5.

Mangan, M.T., and Cashman, K.V., 1996, The structure of basaltic scoria and reticulite and inferences for vesiculation, foam formation, and fragmentation in lava fountains: Journal of Volcanology and Geothermal Research, v. 73, p. 1–18, doi: 10.1016/0377-0273(96)00018-2.

Mangan, M.T., and Sisson, T., 2000, Delayed, disequilibrium degassing in rhyolite magma: Decompression experiments and implications for explosive volcanism: Earth and Planetary Science Letters, v. 183, p. 441–455, doi: 10.1016/S0012-821X(00)00299-5.

Mangan, M.T., Cashman, K.V., and Newman, S., 1993, Vesiculation of basaltic magma during eruption: Geology, v. 21, p. 157–160, doi: 10.1130/0091-7613(1993)021<0157:VOBMDE>2.3.CO;2.

Mangan, M.T., Mastin, L., and Sisson, T., 2004, Gas evolution in eruptive conduits: Combining insights from high temperature and pressure decompression experiments with steady-state flow modeling: Journal of Volcanology and Geothermal Research, v. 129, p. 23–36, doi: 10.1016/S0377-0273(03)00230-0.

Marsh, B.D., 1988, Crystal size distribution (CSD) in rocks and the kinetics and dynamics of crystallization, I, Theory: Contributions to Mineralogy and Petrology, v. 99, p. 277–291, doi: 10.1007/BF00375362.

Massol, H., and Jaupart, C., 1999, The generation of gas overpressure in volcanic eruptions: Earth and Planetary Science Letters, v. 166, p. 57–70, doi: 10.1016/S0012-821X(98)00277-5.

Matthews, S.J., Gardeweg, M.C., and Sparks, R.S.J., 1997, The 1984 to 1996 cyclic activity of Lascar volcano, northern Chile: Cycles of dome growth, dome subsidence, degassing and explosive eruptions: Bulletin of Volcanology, v. 59, p. 72–82, doi: 10.1007/s004450050176.

Mellors, R.A., Waitt, R.B., Jr., and Swanson, D.A., 1988, Generation of pyroclastic flows and surges by hot-rock avalanches from the dome of Mount St. Helens volcano, USA: Bulletin of Volcanology, v. 50, p. 14–25, doi: 10.1007/BF01047505.

Melnik, O., 2000, Dynamics of two-phase conduit flow of high-viscosity gas-saturated magma: Large variations of sustained explosive eruption intensity: Bulletin of Volcanology, v. 62, p. 153–170, doi: 10.1007/s004450000072.

Melnik, O., and Sparks, R.S.J., 1999, Nonlinear dynamics of lava dome extrusion: Nature, v. 402, p. 37–41, doi: 10.1038/46950.

Melnik, O., and Sparks, R.S.J., 2002, Dynamics of magma ascent and lava extrusion at Soufrière Hills Volcano, Montserrat, *in* Druitt, T.H., and Kokelaar, B.P., eds., The eruption of Soufrière Hills Volcano, Montserrat, from 1995 to 1999: Geological Society [London] Memoir 21, p. 153–171.

Melson, W.G., and Saenz, R., 1973, Volume, energy and cyclicity of eruptions at Arenal volcano, Costa Rica: Bulletin of Volcanology, v. 37, p. 416–437.

Minakami, T., 1950, On explosive activities of andesitic volcanoes and their forerunning phenomena: Bulletin of Volcanology, v. 10, p. 59–87.

Moore, H.J., Arthur, D.W.G., and Schaber, G.G., 1978, Yield strength of flows on the Earth, Mars, and Moon, *in* Merrill, R.B., ed., The Moon and the inner solar system: New York, Pergamon, Proceedings of the Ninth Lunar and Planetary Science Conference, p. 3351–3378.

Moore, J.G., Lipman, P.W., Swanson, D.A., and Alpha, T.R., 1981, Growth of lava domes in the crater, June 1980–January 1981: U.S. Geological Survey Professional Paper 1250, p. 541–547.

Orsi, G., Gallo, G., Heiken, G., Wohletz, K., Yu, E., and Bonani, G., 1992, A comprehensive study of pumice formation and dispersal: The Cretaio tephra of Ischia (Italy): Journal of Volcanology and Geothermal Research, v. 53, p. 329–354, doi: 10.1016/0377-0273(92)90090-Z.

Parfitt, E.A., and Wilson, L., 1999, A Plinian treatment of fallout from Hawaiian lava fountains: Journal of Volcanology and Geothermal Research, v. 88, p. 67–75, doi: 10.1016/S0377-0273(98)00103-6.

Polacci, M., Pioli, L., and Rosi, M., 2003, The Plinian phase of the Campanian Ignimbrite eruption (Phlegrean Fields, Italy): Evidence from density measurements and textural characterization of pumice: Bulletin of Volcanology, v. 65, p. 418–432, doi: 10.1007/s00445-002-0268-4.

Sahagian, D.L., and Proussevitch, A.A., 1998, 3D particle size distributions from 2D observations—Stereology for natural applications: Journal of Volcanology and Geothermal Research, v. 84, p. 173–196, doi: 10.1016/S0377-0273(98)00043-2.

Sato, H., Fujii, T., and Nakada, S., 1992, Crumbling of dacite dome lava and generation of pyroclastic flows at Unzen volcano: Nature, v. 360, p. 664–666, doi: 10.1038/360664a0.

Self, S., Wilson, L., and Nairn, I.A., 1979, Vulcanian eruption mechanisms: Nature, v. 277, p. 440–443, doi: 10.1038/277440a0.

Self, S., Kienle, J., and Huot, J.-P., 1980, Ukinrek Maars, Alaska, II, Deposits and formation of the 1977 craters: Journal of Volcanology and Geothermal Research, v. 7, p. 39–65, doi: 10.1016/0377-0273(80)90019-0.

Steinberg, G.S., 1977, On the determination of the energy and depth of volcanic explosions: Bulletin of Volcanology, v. 40, p. 1–5.

Steinberg, G.S., and Babenko, J.I., 1978, Experimental velocity and density determination of volcanic gases during eruption: Journal of Volcanology and Geothermal Research, v. 3, p. 89–98, doi: 10.1016/0377-0273(78)90005-7.

Swanson, D.A., 1990, A decade of dome growth at Mount St. Helens, 1980–90: Geoscience Canada, v. 17, p. 154–157.

Swanson, D.A., and Holcomb, R.T., 1990, Regularities in growth of the Mount St. Helens dacite dome, 1980–1986, *in* Fink, J., ed., Lava flows and domes: Berlin, Springer-Verlag, p. 3–24.

Swanson, D.A., Dzurisin, D., Holcomb, R.T., Iwatsubo, E.Y., Chadwick, W.W., Casadevall, T.J., Ewert, J.W., and Heliker, C.C., 1987, Growth of the lava dome at Mount St. Helens, Washington (USA), 1981–1983, *in* Fink, J., ed., The emplacement of silicic domes and lava flows: Geological Society of America Special Paper 212, p. 1–16.

Toramaru, A., 1990, Measurement of bubble size distributions in vesiculated rocks with implications for quantitative estimation of eruptive processes: Journal of Volcanology and Geothermal Research, v. 43, p. 71–90, doi: 10.1016/0377-0273(90)90045-H.

Touloukian, Y.S., Judd, W.R., and Roy, R.F., 1981, Physical properties of rocks and minerals: New York, McGraw-Hill, 548 p.

Ui, T., Matsuwo, N., Sumita, M., and Fujinawa, A., 1999, Generation of block and ash flows during the 1990–1995 eruption of Unzen volcano, Japan: Journal of Volcanology and Geothermal Research, v. 89, p. 123–137, doi: 10.1016/S0377-0273(98)00128-0.

Voight, B., and Elsworth, D., 2000, Instability and collapse of hazardous gas-pressurized lava domes: Geophysical Research Letters, v. 27, p. 1–4, doi: 10.1029/1999GL008388.

Voight, B., Sparks, R.S.J., Miller, A.D., Stewart, R.C., Hoblitt, R.P., Clarke, A., Ewart, J., Aspinall, W.P., Baptie, B., Calder, E.S., Cole, P., Druitt, T.H., Hartford, C., Herd, R.A., Jackson, P., Lejeune, A.M., Lockhart, A.B., Loughlin, S.C., Luckett, R., Lynch, L., Norton, G.E., Robertson, R., Watson, I.M., Watts, R., and Young, S.R., 1999, Magma flow instability and cyclic activity at Soufrière Hills Volcano, Montserrat: British West Indies: Science, v. 283, p. 1138–1142.

Westrich, H.R., and Eichelberger, J.C., 1994, Gas transport and bubble collapse in rhyolitic magma: An experimental approach: Bulletin of Volcanology, v. 56, p. 447–458, doi: 10.1007/s004450050054.

Wilson, L., 1980, Relationships between pressure, volatile content and ejecta velocity in three types of volcanic explosion: Journal of Volcanology and Geothermal Research, v. 8, p. 297–313, doi: 10.1016/0377-0273(80)90110-9.

Woods, A.W., and Koyaguchi, T., 1994, Transitions between explosive and effusive eruptions of silicic magmas: Nature, v. 370, p. 641–644, doi: 10.1038/370641a0.